In-Situ STM Study of Te UPD Layers on Low Index Planes of Gold

Brian E. Hayden* and Iris S. Nandhakumar

Department of Chemistry, The University, Southampton SO17 1BJ, United Kingdom

Received: February 14, 1997; In Final Form: April 26, 1997[⊗]

The structure of well-ordered atomic layers of underpotentially deposited (UPD) tellurium on Au(110), Au(100) and Au(111) was studied by in-situ scanning tunneling microscopy (STM). A series of largely commensurate structures is observed, with a close correspondence between coverages obtained from the STM images and the cyclic voltammetry assuming complete discharge of Te^{4+} during adsorption. A linear dependence of the UPD peak current and the peak potential with the square root of the scan rate is observed indicating that the adsorption phase transition is associated with a two-dimensional, instantaneous nucleation process. The same structures are observed in sulfuric acid and perchloric acid supporting electrolyte. The first UPD structure formed on Au(111) corresponds to a pseudohexagonal packing of Te (0.42 ML) (ML = monolayer) in a single domain superlattice structure with missing atom defects. The superlattice cell is $(3\sqrt{7} \times 3\sqrt{7})R19°$ with respect to the constituent Te atom hexagonal cell and is consistent with the (12×12) structure on Au(111) reported previously. The second UPD structure on Au(111) is a pseudo-morphic (1×1). The Te-substrate interaction favors site specific adsorption, and dipolar repulsion within low-coverage layers is responsible for the open packing.

1. Introduction

Epitaxial films of II−VI semiconductor compounds such as cadmium telluride are promising candidates in solar cell applications and infrared detection.[1] A major thrust of recent research has been dedicated to studying their formation by cathodic electrodeposition from aqueous solutions[2−20] as this method provides an attractive, low cost, ambient temperature approach to the fabrication of these devices. Most of the previous Cd/Te electrodeposition studies, however, have resulted in amorphous and polycrystalline deposits with extensive grain boundaries leading to an increased resistivity of these materials.[21] Long-range order through epitaxy and the creation of sharp phase boundaries, are hence particularly important goals. Recently Stickney and co-workers have developed a new technique for the preparation of compound semiconductors, which they refer to as electrochemical atomic layer epitaxy (ECALE).[22−23] This involves the alternate deposition of the constituent elements by electrochemical reduction or oxidation of ionic precursors in the liquid phase to form a semiconductor compound. Epitaxial growth is achieved by using UPD to limit the adsorption to sub-monolayer and monolayer coverages.

The aim of this study is to investigate the atomic arrangement of various UPD structures of tellurium on the low index planes of gold by monitoring their nucleation and growth in-situ as a first step toward arriving at an atomic level description of Cd/Te epitaxy. Te UPD layers on gold single crystal surfaces have been the subject of ex-situ low-energy electron diffraction (LEED) investigation following transfer from the electrochemical environment.[24] Ex-situ scanning tunneling microscopy (STM) studies have also been reported[25] for the Te layers and alternate deposition of Te and Cd, on single-crystal gold surfaces involving transfer of the substrate (emersion) from solution with concomitant loss of potential control. There are numerous limitations associated with having to remove the electrode from solution.[26,27] This in-situ STM study with the associated voltammetry allows a direct comparison with the structures obtained from ex-situ studies, and some emphasis has been placed on elucidating the question of whether coadsorbed anions from the supporting electrolyte plays a role in this particular system as it is known from a number of studies that anions can have a major impact on the formation of UPD structures.[28]

2. Experimental Section

In-situ STM studies were performed with a commercial Topometrix TMX 2010 equipped with a bipotentiostat for electrochemical STM. The tips employed in this study were made of tungsten, electrochemically etched from a 0.25 mm diameter wire in 2 M NaOH and coated with Apiezon wax to reduce the surface area in contact with the electrolyte. The tip potential could be controlled independently of the working electrode potential, and it was generally held between −0.2 and 0 V vs SCE resulting in Faradaic currents of less than 100 pA. All STM images were recorded in the constant-current mode with tunneling currents ranging from 2−5 nA and are shown as top views with different heights colored in different shades of grey; lighter shades correspond to higher points. The working electrodes were either single gold crystal discs, 14 mm in diameter and 2 mm thick, or 200 nm thick evaporated gold films onto Tempax glass (AF45, Berliner Glas KG). These films had a 2 nm thick chromium undercoating for better adhesion of the gold film to the glass. Before each experiment, the gold on glass films were flame annealed in a hydrogen flame for about 2−3 min at yellow heat, producing large regions of atomically flat (111) terraces often extending over hundreds of nanometres. The gold single crystal electrodes were mechanically polished (MaTeck) down to 0.03 μm and subsequently electrochemically polished in 1 M perchloric acid to remove mechanical damage. Before each experiment the gold single-crystal electrode was subjected to flame annealing at red heat in a Bunsen flame for a total of 5−10 min, depending on the surface condition. After each experiment the crystal was cleaned by anodic polarization by growing a visible thick oxide layer, followed by dissolution of the oxide in diluted HCl. The electrolyte was prepared from H_2SO_4 (Aldrich, suprapure) and TeO_2 (Aldrich, p.a.) with water from a Milli-Q purification system.

The solution was not deaerated with nitrogen prior to the experiment because the electrochemical cell was open to air.

[⊗] Abstract published in *Advance ACS Abstracts,* August 15, 1997.

S1089-5647(97)00565-8 CCC: $14.00

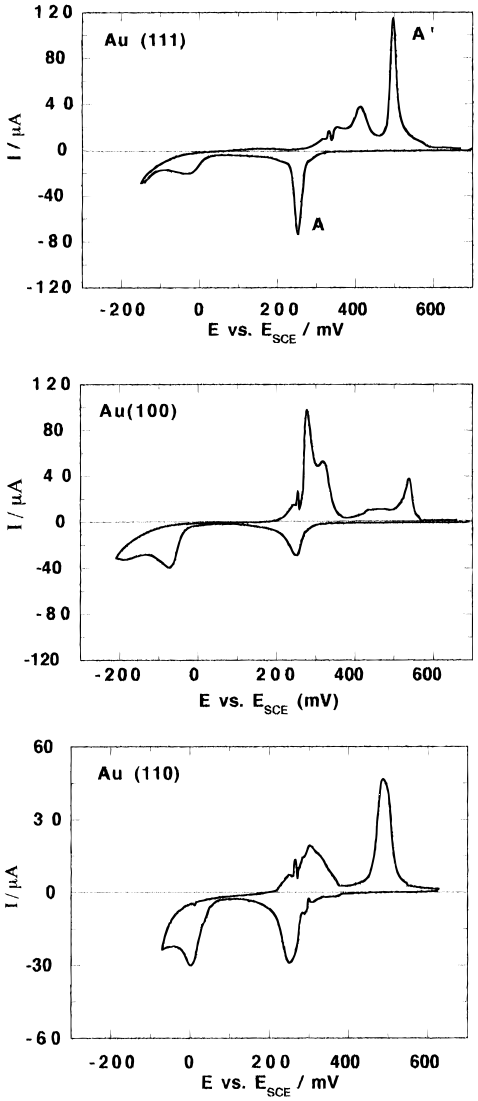

Figure 1. Cylic voltammograms recorded in the STM cell for the low index planes of gold: in 0.4 mM TeO_2 and 10 mM H_2SO_4, scan rate 10 mV s^{-1}.

Although an electrooxidized gold wire was used as a reference electrode, all electrode potentials are reported with respect to the saturated calomel electrode. A gold or platinum wire directly immersed in the cell served as a counter electrode. The STM piezoelectric tube scanner was calibrated in the *x* and *y* surface plane using the $(\sqrt{3} \times \sqrt{3})R30°$ structure of Cu on Au(111) as a standard, and in *z* (surface normal direction) by imaging the gold atomic step height (2.46 Å). All images presented are unfiltered unless otherwise indicated in the figure caption.

3. Results

Figure 1 shows typical cyclic voltammograms for the underpotential deposition (UPD) of tellurium on the low index planes of gold from solutions containing 0.4 mM TeO_2 + 10 mM H_2SO_4 recorded in the STM cell. Similar voltammograms were obtained in perchloric acid electrolyte (0.4 mM TeO_2 + 10 mM $HClO_4$). In each case the first potential scan is depicted. The voltammetry was found to be stable and reversible, persisting over many cycles, suggesting that alloy formation between Te and Au in the region of potential investigated does not occur. The results are in good agreement with what has been reported in the literature,[25] although the peaks in Figure 1 are more prominent and sharper, which we interpret as indicating a well prepared surface. The underpotential deposition of tellurium takes place (Figure 1) in two well-separated steps occurring at potentials of approximately 0.250 V and −0.034 V vs SCE respectively on all the gold surfaces investigated, and prior to the onset of tellurium bulk deposition at −0.140 V. These deposition waves are referred to as the first and second UPD peaks respectively throughout. There is a significant potential hysteresis between the first UPD deposition and stripping peaks (0.250 V and 0.500 V). This implies a kinetic hindrance in the formation and/or dissolution of the UPD phase. This is also an indication[29] that a first-order phase transition may be associated with the process. The sharpness of the respective current peaks and the high current densities associated with them provide additional evidence for an underlying first-order phase transition. To investigate this behavior further the scan rate was varied and the peak currents and potentials of the first UPD peak pair on Au(111) (A/A′ in Figure 1) were plotted as a function of the square root of the scan rate. A linear dependence of the UPD peak current and the peak potential with the square root of the scan rate is predicted[30] if the observed phase transition is associated with a two-dimensional, instantaneous nucleation process. A plot of this dependency is shown in Figure 2, which agrees well with the predicted behavior.

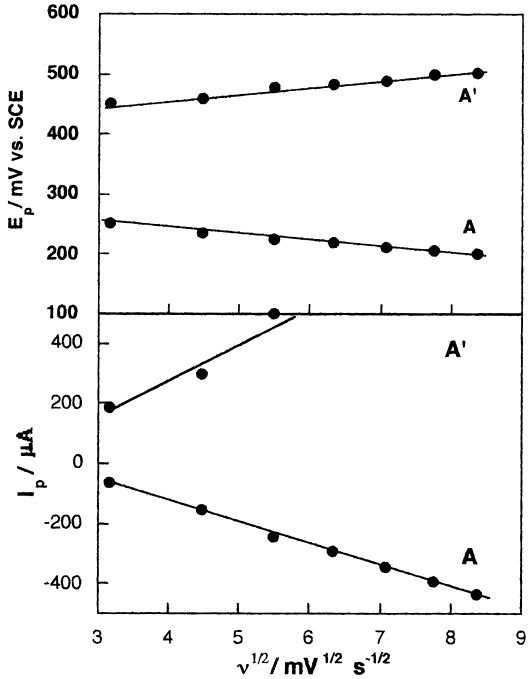

Figure 2. Peak potentials (E_p) and peak currents (I_p) of peaks A and A′ of cyclic voltammogram for Au (111) (as indicated in Figure 1) plotted vs the squareroot of the scan rate.

We monitored the underpotential deposition of tellurium on the low index planes of gold by in-situ STM in two electrolytes: sulfuric acid, in which the anions are known to be strongly specifically adsorbing, and perchloric acid, in which they are weakly adsorbed,[31] On the Au(111) surface cycling through the first tellurium UPD peak gave rise to images as shown in Figure 3 (top and bottom). The potential was held at 0.100 V SCE, in the potential region between the the first and second Te UPD peaks, during the scanning of the image. The STM images evidence a large hexagonal superlattice structure with a unit cell dimension of 34.6 ± 0.3 Å corresponding to approximately a (12 × 12) periodicity with respect to the Au(111) substrate, and with a regular pattern of point defects. By taking cross sections through the unit cell it could be established that these

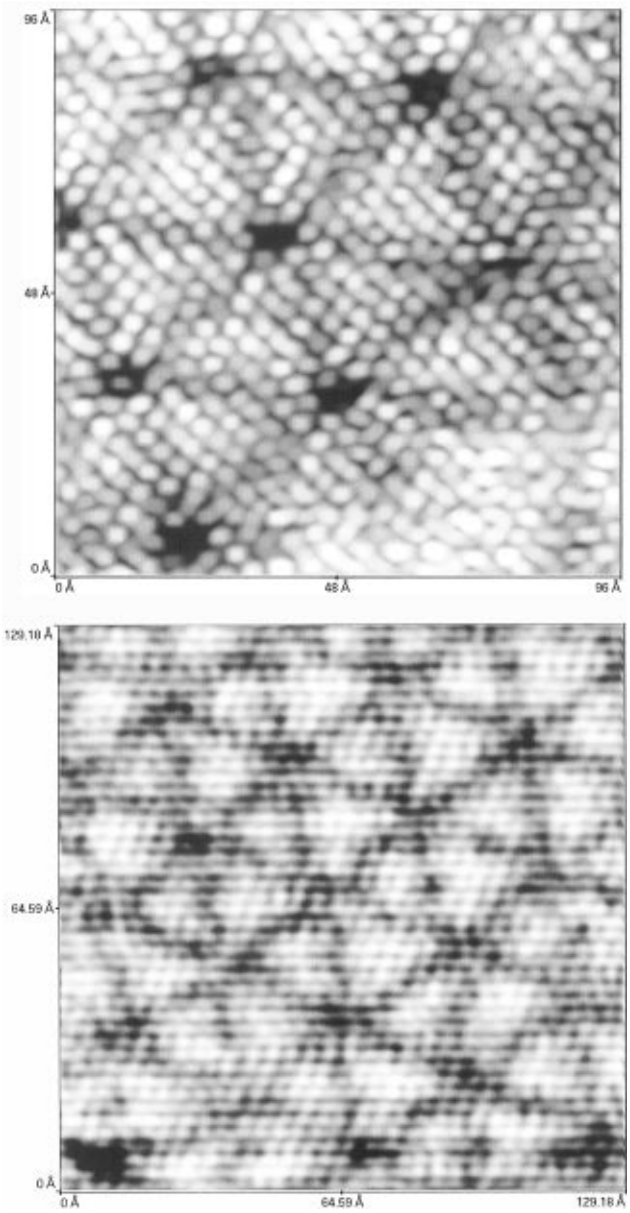

Figure 3. STM micrographs. Top and bottom following first Te UPD deposition on Au (111): (a) (12 × 12) overlayer structure and (b) larger scan area image of (a).

apparent point defects generally correspond to missing atoms. The atom−atom spacing deduced from these images, as well as from the corresponding two-dimensional Fourier transform (Figure 4), is on average 4.4 Å. The measured average atomic corrugation is 0.5 Å and varies along the rows with values ranging from 0.3−0.7 Å. The structure was found to be independent of the supporting electrolyte and formed extensive networks on large terrace regions, often extending over several hundreds of angströms (Figure 3b). A tellurium coverage for the first UPD peak of 0.42 ± 0.01 ML was extracted from an analysis of the STM micrographs, assuming that each of the apparent atoms (Figure 3) corresponds to adsorbed tellurium. The coverage was also estimated from the total charge associated with the first UPD deposition and stripping peaks (∼370 μC/cm^{-2}) after deduction of the double-layer charging current. Assuming that the effective surface area of the crystal is equal to its cross-sectional geometric area (a surface roughness of unity), the number of substrate atoms was 1.39×10^{15} atoms cm^{-2}, and the charge transfer associated with the deposition was 4e$^-$ atom^{-1},[32] the coverage was found to be 0.42 ± 0.02 ML.

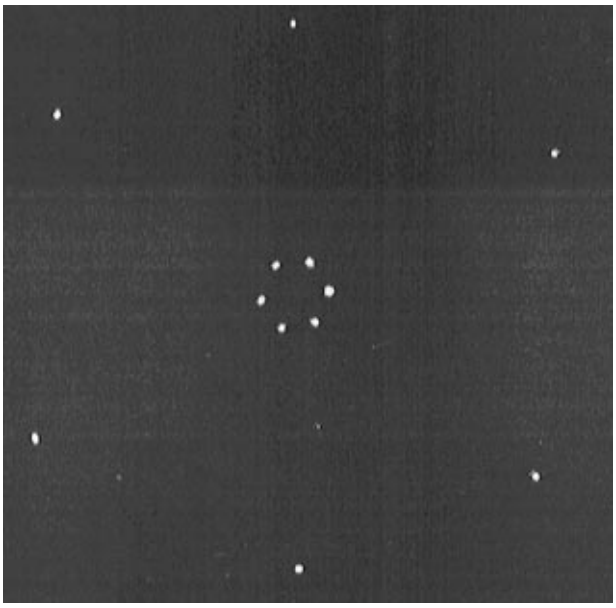

Figure 4. Two-dimensional Fourier transform of (b) showing the two hexagons due to the atomic and the superstructure periodicity. The two hexagons are rotated against each other by 19° ± 2°.

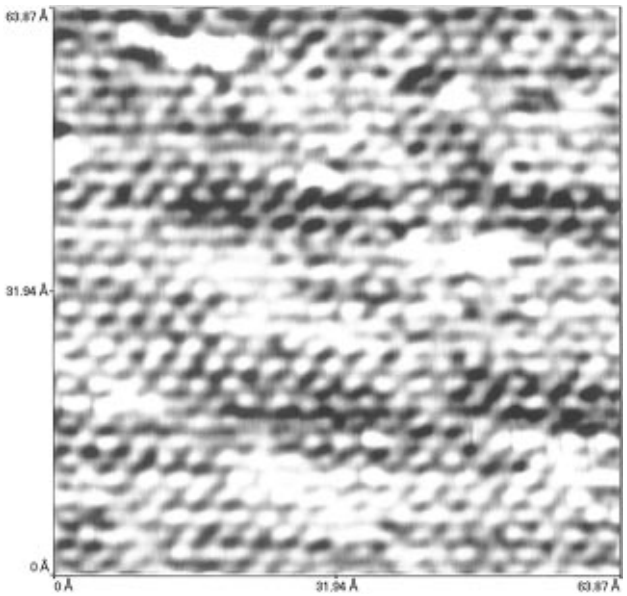

Figure 5. STM micrograph recorded after deposition through the second Te UPD peak on Au (111) showing a pseudomorphic (1 × 1) overlayer. The image was filtered by 2-D Fourier transform.

Figure 4 shows the two-dimensional Fourier transform spectrum of the image shown in Figure 3(bottom) and exhibits two hexagons. These correspond to an atomic periodicity of the tellurium of 4.4 ± 0.3 Å and a periodicity for the long-range superstructure of 34.6 ± 0.3 Å. The two hexagons are rotated by an angle of approximately 19 ± 2° with respect to one another. The apparent distortion of the hexagonal Te adlayer structure evident in the Fourier transform is associated with thermal $x-y$ drift during scanning. The long range superstructure (Figure 3 (bottom)) corresponds to a ($3\sqrt{7} \times 3\sqrt{7}$)R19.16 unit cell with respect to the close-packed Te unit cell.

A change in the overlayer structure was detected following deposition through the second UPD peak, and the resulting images are shown in Figure 5. The potential was held at −0.092 V SCE during the scanning of the images. The measured nearest neighbour spacing in this image is 3.1 ± 0.2 Å. This

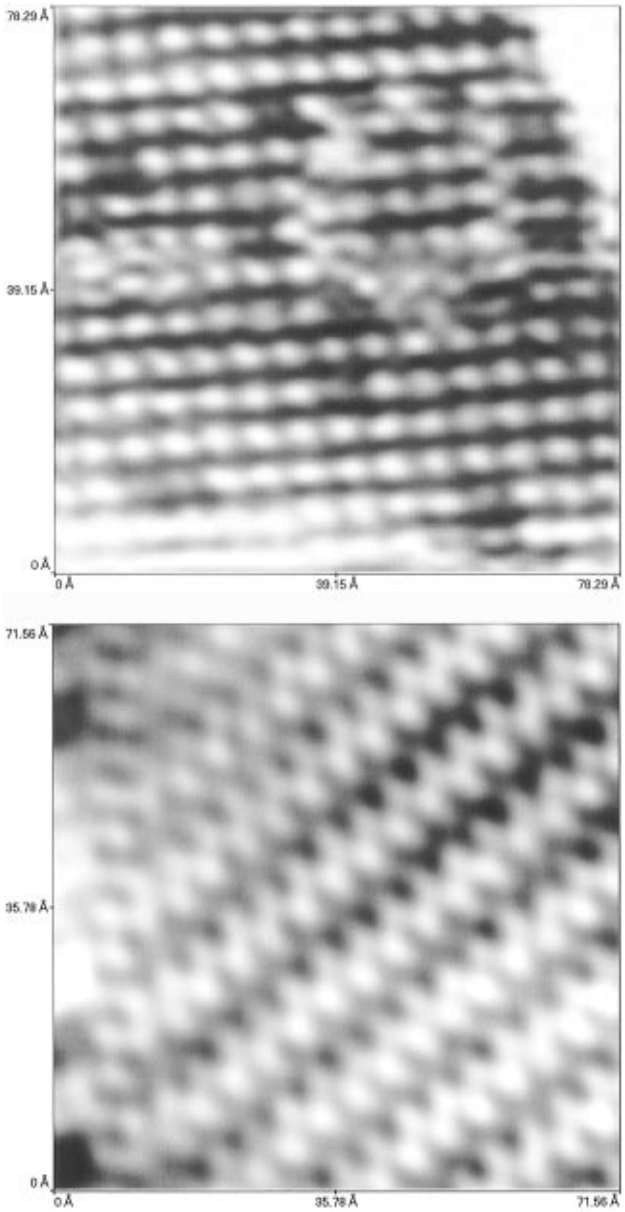

Figure 6. STM micrographs following deposition of first (top) and second Te UPD (bottom) on Au (100): (top) a c(2 × 2) and a (bottom) (2 × $\sqrt{10}$) overlayer structure. The image at the bottom was 2-D FT filtered.

spacing is close to the lattice constant of the Au(111) substrate (2.89 Å). The coverage determined from the STM image was found to be 0.90 ± 0.01 ML (ML = monlayer), and from the total integrated charge of the first and second UPD peaks in the corresponding cyclic voltammogram (Figure 1) was estimated to be 0.93 ± 0.02 ML.

STM images corresponding to the underpotentially deposited tellurium layers on the Au(100) and the Au(110) plane are depicted in Figures 6 and 7 respectively. The images were scanned at a potential of 0.10 V for the first UPD layer and −0.10 V for the second. The overlayer structure associated with the first UPD Te layer on the Au(100) shown in Figure 6(top) corresponds to a square unit cell of dimension 5.61 ± 0.2 Å and 0.25 ML coverage. We were unable to image a significantly more densely packed overlayer for the second UPD structure, which according to the integrated charge should have had a coverage of 0.71 ML. Instead we observed a lower coverage structure (Figure 6(bottom)) with a unit cell dimension of 5.35 ± 0.2 Å × 10.7 ± 1.2 Å and coverage of 0.3 ML. The overlayer structure associated with the first UPD Te layer on

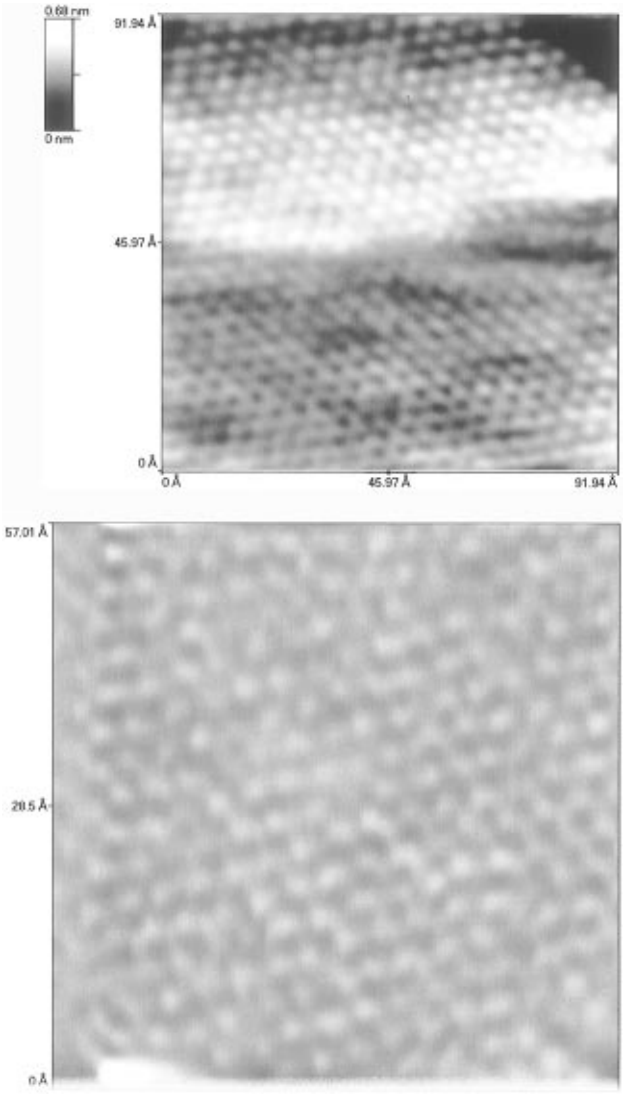

Figure 7. STM images obtained after deposition through the first (top) and second (bottom) Te UPD peak on Au (110). (top) c(2 × 8) and (bottom) c(2 × 6) overlayer structures. The images in both cases were filtered using a 2-D Fourier transform.

TABLE 1

Au crystal face	UPD peak	coverage /ML from STM	coverage /ML from charge	overlayer structure
(100)	first	0.26 ± 0.01	0.24 ± 0.01	(2 × 2)
(100)	second	0.30 ± 0.01	0.71 ± 0.02	(2 × $\sqrt{10}$)
(110)	first	0.61 ± 0.01	0.61 ± 0.02	c(2 × 8)
(110)	second	0.81 ± 0.01	0.82 ± 0.02	c(2 × 6)
(111)	first	0.42 ± 0.01	0.42 ± 0.02	(12 × 12)
(111)	second	0.90 ± 0.01	0.93 ± 0.02	(1 × 1)

the Au(110) shown in Figure 7(top) corresponds to what appears to be a distorted hexagonal unit cell with a mean Te−Te distance of 4.6 ± 0.2 Å and a coverage of 0.61 ML coverage (Table 1). Registry with the rectangular unit cell of Au(110) indicates a c(2 × 8) structure with a unit cell of dimension 8.35 ± 0.3 Å × 23.93 ± 0.8 Å, observed in previous ex-situ LEED measurements for this structure.[24] A second more densely packed and distorted hexagonal structure with an average Te−Te distance of 4.3 ± 0.2 Å is observed with a coverage of 0.81 ML for the second UPD layer (Figure 7(bottom)). This structure exhibits a registry with the Au(110) consistent with the c(2 × 6) structure observed previously in ex-situ LEED measurements.[24] The coverages determined from these images, as well as from the corresponding cyclic voltammograms (Figure 1) were found

to be in close agreement, as was found for structures on Au(111). The exception to this was the densely packed overlayer for the second UPD structure on Au(100), which according to the integrated charge should have had a coverage of 0.71 ML. Instead we observed a lower coverage structure with a unit cell dimension of 5.35 ± 0.2 Å × 10.7 ± 1.2 Å and coverage of 0.3 ML, although there were indications of a higher coverage structure which decayed quickly under the influence of the tip even under potential control. Images of the second UPD structures on Au(111) and Au(110) were also much more difficult to obtain than the first UPD structures.

4. Discussion

We suggest that the overlayer structures observed by STM in this study correspond to the actual structure of adsorbed Te atoms on the gold surfaces, and are not associated with specific anion adsorption. The structures appear insensitive to the supporting electrolyte, and the coverages estimated from the structures themselves in STM and coverages estimated from the cyclic voltammetry show a close correspondence.

The first UPD structure observed on Au(111) comprises close packed Te atoms (Figure 3a) with an average interatomic spacing of 4.4 ± 0.2 Å. The Te atoms must be displaced slightly from positions expected from a perfect hexagonal overlayer to produce the $(3\sqrt{7} \times 3\sqrt{7})R19.16°$ superlattice defect structure (Figure 3(bottom)) (defined with respect to the averaged hexagonal Te unit cell). This superlattice is likely to be commensurate with the Au(111) lattice, with incommensurate Te atoms on the Au(111) surface within the larger unit cell. Since we are unable to image the substrate atoms in the presence of the supporting electrolyte, we are unable to directly measure the relationship of the superlattice structure with respect to the Au(111) unit cell, although this is discussed further below.

The average interatomic spacing of the constituent Te atoms of 4.4 ± 0.2 Å corresponds to a local structure which is significantly more open packed than that corresponding to the bulk tellurium hcp (0001) basal plane (Te−Te distance of 2.86 Å). The stabilization of such openly packed metal structures in the underpotential regime can be attributed to the influence of coadsorbed anions. This has been verified in a number of systems such as Cu and Ag on Au(111) where it has been established that co-adsorbed anions determine the observed underpotential structures.[33] In other cases, such as Hg and Bi on Au(111),[34−35] the anions were found to have little effect on either the observed UPD structures or on the associated cyclic voltammograms. To explain this phenomenon, it was suggested[36] that the apparent repulsive interactions between the adatoms originate from an incomplete discharge of the adatom. This would result in a partial charge on the UPD metal and strong repulsive Coulombic forces.

The insensitivity of the open packed Te structures on the gold surfaces (Figures 3, 6, and 7) and the associated voltammetry (Figure 1) to the supporting electrolyte suggests that the overlayers are not stabilised primarily by coadsorbing anions within the overlayer structure. The correspondence of the coverages obtained for the Te structures from the integrated charge in voltammetry (if one assumes an overall $4e^-$ process) and coverages obtained from the STM images for all the surfaces investigated suggests that complete discharge of the Te^{4+} ion takes place on adsorption. This observation is in agreement with a number of other studies in which it was concluded that the initial step in the electroreduction of $HTeO_2^+$ is a $4e^-$ reduction of Te^{4+} to $Te°$.[37] Therefore, residual Coulombic charge in the adsorbate layer is unlikely to be responsible for the apparent repulsive interactions in the open packed UPD layers. We suggest that the open packing is a result primarily of dipolar interactions resulting from a strong bonding interaction between Te and Au in the first UPD layer. Although largely covalent in nature, one may expect significant charge separation simply on the grounds of differences in electronegativity. This limit is most akin to that exhibited at the gas−solid interface where such interactions can result in open packed commensurate and semi-commensurate overlayers of metals on metal surfaces such as Bi on platinum.[38−40] The strong intrinsic interaction expected between Te and Au is consistent with such a model for this adsorption system, and there is evidence that Te in the first UPD structure modifies the surface density of the bound electrons of gold.[41] Such a dipole interaction in a strongly chemisorbing system is also consistent with the observation of complete overall discharge of the Te^{4+} ion on adsorption and an insensitivity to supporting electrolyte. It also accounts for the influence of the Au(111) lattice in distorting a hexagonally packed Te layer to produce a long range defect structure. Similar interactions, and therefore structures, would be expected in the absence of the electrolyte at the gas−solid interface. We are, however, not aware of any UHV studies of vapor-deposited Te on Au single crystal surfaces. Sulfur adsorption on Au(111) provides a comparable adsorption system where the open packed commensurate UPD structure[42] is the same as that expected at the gas−solid interface. A strong chemisorption interaction for Te on gold is also in line with the observation of commensurate structures for the first UPD layers on the Au(100) and Au(110) surfaces (below), and the fact that the structures we observe under potential control are also stable in air or following vacuum transfer.[24,25]

We were unable to observe the structure of the underlying Au substrates at any potential (including those more positive than the first UPD peaks) with the UPD electrolyte above the surface. This is similar to the case of Hg on Au(111) where the substrate corrugation could not be observed in AFM in the presence of the UPD electrolyte.[33] A large overlayer lattice was also observed by LEED for the first Te UPD layer on Au(111) following transfer to vacuum, where a (12 × 12) was observed.[24,43] A substrate registry of (12 × 12) is consistent with the unit cell spacing observed for the in-situ STM structure on Au(111) (Figure 3), both in the lattice size (a (12 × 12) corresponds to 34.68 Å) and the observation of a single domain of the defect structure in all images obtained. However, there appears to be some difference between the Te coverage obtained previously of 0.33 ML,[24] and that obtained in this study. Figure 8 shows a superposition of the $(3\sqrt{7} \times 3\sqrt{7})$R19.16 defect structure as a (12 × 12) superlattice on Au(111). Two adsorption models are presented. In the first (Figure 8a) we have assumed that the corner defect sites correspond to missing Te atoms at on-top sites on the substrate. There appear to be missing Te atoms at the corners of the superlattice structure (Figure 3a). In some instances, however, we do appear to observe a Te atom in the corner sites, and one possibility is that at these positions Te is adsorbed in 3-fold hollow sites. Figure 8b corresponds to such a (12 × 12) registry. We have assumed in both models that high coordinate sites are favored by Te, and there is no reconstruction of the Au(111) substrate. The models are shown for a perfect hexagonal Te overlayer, although there is probably some relaxation of the Te toward the high coordinate (3-fold hollow) sites within the superlattice. The second model (Figure 8b) appears to have the advantage that, even in their unrelaxed positions, the Te atoms are adjacent to high coordinate sites within the superlattice unit cell. It is difficult to account for the differences in the coverage and hence associated adsorption model suggested for this structure previ-

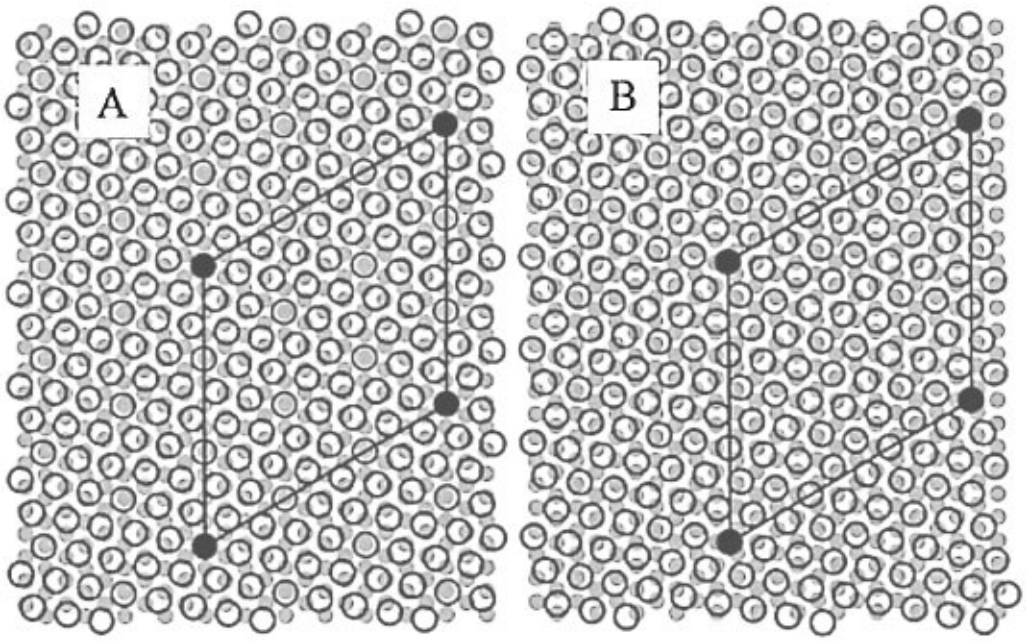

Figure 8. Proposed adsorption site models for the (12 × 12) superlattice structure observed on Au (111) following first Te UPD deposition peak with a coverage of 0.42 ML and a Te−Te spacing of 4.47 Å. Assuming corner defects are (A) missing Te atoms in atop positions and (B) Te atoms adsorbed in 3-fold hollow sites.

ously[24,25] and the structure obtained here (Figure 8), particularly in the light of the similarity in the long range periodicity. We note that the first UPD Te structure we observe on Au(111) (Figure 3) we are also able to image following immersion of the sample, rinsing, and reestablishment of potential control in a cadmium containing electrolyte (but before Cd UPD deposition) in Cd/Te growth studies.[44]

As we take the deposition through the second UPD peak we observe another hexagonal structure with a spacing that is close to that expected for the bare Au(111) lattice. This would imply a pseudomorphic (1 × 1) tellurium overlayer for the second UPD structure, which is theoretically possible given the Te−Te spacing of 2.86 Å for the most densely packed (0001) plane of the tellurium bulk lattice. This structure is also consistent with the derived coverage of 0.93 ML (Table 1). The structure differs significantly from that measured by ex-situ methods[24,25] where the second UPD structure was found to be a (3 × 3) with a coverage of 0.44 ML. This reflects a lack of stability, and concomitant increase in reactivity for Te in the second UPD structure. Depolarisation of the bonding at high coverages will result in a more metallic and reactive adsorbate layer. Indeed, under ex-situ conditions the second (3 × 3) UPD structure quickly degraded to produce the lower coverage (12 × 12) structure in STM.[25] The depolarization associated with the formation of the significantly less stable 2nd UPD structure is also reflected in recent SHG results where a difference in the optical response of the 1st and 2nd UPD layers on polycrystalline gold is interpreted as a difference in the Te−Au interaction.[41]

STM images corresponding to the first UPD Te layer on the Au(100) in Figure 6 corresponds to a square unit cell of dimension 5.61 ± 0.20 Å and 0.25 ML coverage (Table 1). This is consistent with the observation of a (2 × 2) overlayer structure reported earlier under ex-situ conditions and in-situ AFM measurements.[45] We were unable to image a significantly more densely packed overlayer for the second UPD structure, which according to the integrated charge should have had a coverage of 0.71 ML. Instead we observed a lower coverage structure with a unit cell dimension of 5.35 ± 0.2 Å × 10.7 ± 1.2 Å and coverage 0.3 ML corresponding closely to a previously observed (2 × $\sqrt{10}$) structure in the ex-situ measurements.[24,25] However, we observe the (2 × $\sqrt{10}$) only after the observation of a more densely packed structure in STM which quickly degrades. Under the tunneling conditions which had to be chosen for stable in-situ imaging employing a W tip, significant tip−surface interaction was probably responsible for the degradation of the structure even under potential control. This structure is the subject of continued investigation. We note that a higher coverage structure (corresponding to a ($\sqrt{2}$ × $\sqrt{5}$)*R*45°) was also observed to degrade in ex-situ measurements. We also see no evidence for a ($\sqrt{2}$ × $\sqrt{2}$)*R*45° structure reported in AFM measurements.[45] It therefore appears from the variety of results obtained for the second UPD structure, the discrepancy of the coverage and observed STM image (table 1), and the degradation of the structures by tip interaction, that, while the first UPD structure is rather stable on Au(100), the second UPD structure is significantly less stable.

STM images corresponding to the first UPD Te layer on the Au(110) in Figure 7a corresponds to a uniaxially distorted hexagonal structure with an average Te−Te spacing of 4.6 ± 0.2 Å and a coverage of 0.61 ML (Table 1). The structure is therefore consistent with the c(2 × 8) observed in ex-situ LEED and the associated real space model for the overlayer:[24] The rectangular unit cell (8.35 ± 0.30 Å × 23.93 ± 0.80 Å) is indicated in Figure 7a. The second UPD structure (Figure 7b) corresponding to a coverage of 0.81 ML appears more hexagonal and is also consistent with the observation of a c(2 × 6) in LEED.[24] The associated rectangular unit cell (8.29 ± 0.20 Å × 17.89 ± 0.60 Å) is shown in Figure 7b. However, there are no indications of dimer formation[24] in this layer and it appears to be created through a homogeneous uniaxial compression along the <110> azimuth of Au(110) of the first UPD structure. It therefore appears that there is a good correlation between the ex-situ and in-situ structures observed for Te on Au(110), although we note again that the second UPD structure is significantly more difficult to image even under potential control.

5. Conclusions

We present the first in-situ investigation of well ordered atomic layers of underpotentially deposited (UPD) tellurium on Au(110), Au(100), and Au(111). A series of largely commensurate structures is observed, with a close correspondence between coverages obtained from the STM images and the cyclic voltammetry assuming complete discharge of Te^{4+} during adsorption. A linear dependence of the UPD peak current and the peak potential with the square root of the scan rate is observed indicating that the adsorption phase transition is associated with a two-dimensional, instantaneous nucleation process. The same structures are observed in sulfuric acid and perchloric acid supporting electrolyte. The first UPD structure formed on Au(111) corresponds to a pseudohexagonal packing of Te (0.42 ML) in a single domain superlattice structure with missing atom defects. The superlattice cell is $(3\sqrt{7} \times 3\sqrt{7})R19°$ with respect to the constituent Te atom hexagonal cell, and is consistent with the (12×12) structure on Au(111) reported previously,[24] although the real space model for the structure is somewhat different to that suggested. The second UPD structure on Au(111) is a pseudomorphic (1×1) and differs from that observed in ex-situ measurements.[24,25] On Au(110) and Au(100) we observe structures similar to those observed in ex-situ measurements with the exception of the second UPD structure on Au(110). The Te-substrate interaction favors site specific adsorption, and dipolar repulsion within low-coverage layers is responsible for the open packing.

Acknowledgment. The authors gratefully acknowledge helpful discussions with Professor Roger Parsons, Professor John L. Stickney, and the invaluable support from Professor Dieter M. Kolb regarding the STM instrumentation. We also thank the EPSRC for financial support under Grant GR/H58582.

References and Notes

(1) Zanio, K. In Willardson, R. K., Beer, A. C., Eds.; *Semiconductors and Semimetals*; Academic Press: New York, **1978**; Vol. 13, p 197.
(2) Danaher, W. J., Lyons, L. E. *Nature* **1978**, *271*, 139.
(3) Danaher, W. J.; Lyons, L. E. *Aust. J. Chem.* **1983**, *36*, 1011.
(4) Danaher, W. J.; Lyons, L. E. *Aust. J. Chem.* **1984**, *37*, 689.
(5) Lyons, L. E.; Morris, G. C.; Horton, D. H.; Keyes, J. G. *J. Electroanal. Chem.* **1984**, *168*, 101.
(6) Labres, J. *J. Electrochem. Soc.* **1984**, *131*, 464.
(7) Battacharya, R. N.; Rajeshwar, K. *J. Electrochem. Soc.* **1984**, *131*, 2032.
(8) Battacharya, R. N.; Rajeshwar, K.; Noufi, R. N. *J. Electrochem. Soc*. **1985**, *132*, 732.
(9) Mori, E.; Rajeshwar, R. *J. Electroanal. Chem.* **1989**, *258*, 415.
(10) Mishra, K. K.; Rajeshwar, K. *J. Electroanal. Chem.* **1989**, *273*, 169.
(11) Takahashi, M.; Uosaki, K.; Kita, H. *J. Electroanal. Chem.* **1984**, *131*, 2304.
(12) Takahashi, M.; Uosaki, K.; Kita, H. *J. Appl. Phys.* **1984**, *55*, 3879.
(13) Uosaki, K.; Takahashi, M.; Kita, H. *Electrochim. Acta* **1984**, 279.
(14) Gerritsen, H. J. *J. Electrochem. Soc.* **1984**, *131*, 136.
(15) Carbonelle, P.; Labar, C.; Lamberts, I. *Analysis* **1987**, *15*, 286.
(16) Sella, C.; Boncorps, P.; Vedel, J. *J. Electrochem. Soc.* **1986**, *133*, 2043.
(17) Maurin, G.; Solorza, O.; Takenouti, H. *J. Electroanal. Chem.* **1986**, *202*, 323.
(18) Cowache, P.; Lincot, D.; Vedel, J. *J. Electrochem. Soc.* **1989**, *136*, 1646.
(19) Touskova, J.; Kindl, D.; Tousek, J. *Solar Energy Mat.* **1989**, *18*, 377.
(20) Sanyal, G. S.; Mondal, A.; Mandal, K. C.; Gosh, B.; Sata, K.; Mukherjee, M. K. *Solar Energy Mater.* **1990**, *20*, 395.
(21) Chartier, P.; Ba, B.; Ebothe, J.; Vante, N. A.; Cong, H. N. *J. Electroanal. Chem.* **1982**, *138*, 381.
(22) Gregory, B. W.; Stickney, J. L. *J. Electroanal. Chem.* **1991**, *300*, 543.
(23) Gregory, B. W.; Suggs, D. W.; Stickney, J. L. *J. Electrochem. Soc.* **1992**, *138*, 1279.
(24) Suggs, D. W.; Stickney, J. L. *J. Phys. Chem*., **1991**, *95*, 10056.
(25) Suggs, D. W.; Stickney, J. L. *Surf. Sci.* **1993**, *290*, 375.
(26) Weaver, M. J.; Gao, X. *Ann. Rev. Phys. Chem.* **1993**, *44*, 459.
(27) Lipkowski, J., Ross, P. N., Eds. *Frontiers of Electrochemistry*; VCH: New York, 1993; Vol. 2. (Structure of Electrified Interfaces).
(28) Kolb, D. M. *Schering Lecture's Publications* **1991**, *2*.
(29) Hölzle, M. H.; Retter, U.; Kolb, D. M. *J. Electroanal. Chem.* **1994**, *371*, 101.
(30) Bosco, E.; Rangajaran, S. K. *J. Electroanal. Chem.* **1981**, *129*, 25.
(31) Angerstein-Kozlowska, H.; Conway, B. E. *Electrochim. Acta* **1986**, *31*, 1051.
(32) Pacicke, M. P. R.; Knaster, M.; Kröger, S. F. *J. Electrochem. Soc.* **1978**, *125*, 566.
(33) Shi, Z.; Lipkowski, J. *J. Electroanal.Chem.* **1994**, *365*, 303; **1994**, *364*, 289.
(34) Chen, C.-H.; Gewirth, A. A. *J. Am. Chem. Soc.* **1992**, *114*, 451.
(35) Chen, C.-H.; Gewirth, A. A. Ultramicroscopy **1992**, *42*−*44*, 437. Chen, C.-H.; Kepler, K. D.; Gewirth, A. A.; Ocko, B. M.; Wang, J. *J. Phys. Chem.* **1993**, *97*, 2790. Chen, C.-H.; Gewirth, A. A. *J. Am. Chem. Soc.* **1992**, *114*, 5439.
(36) Chen, C.-H.; Gewirth, A. A. *Phys. Rev. Lett.* **1992**, *68*, 1571.
(37) Conway, B. E.; Norton, M. L.; Stickney, J. L. *J. Electroanal. Chem.* **1990**, *293*, 85. Sarala,Y.; Reddy, S. J. *J. Electroanal. Chem.* **1986**, *214*, *179*. Mori, E.; Baker, C. K.; Reynolds, J. R.; Rajeshwar, K. *J. Electroanal. Chem.* **1988**, *252*, 441.
(38) Paffet, M. T.; Campbell, C. T.; Taylor, N. T. *J. Chem. Phys.* **1986**, *85*, 6176.
(39) Godfrey, D. C.; Hayden, B. E.; Murray, A. J.; Parsons, R.; Pegg, D. J. *Surf. Sci.* **1993**, *294*, 33.
(40) Hayden, B. E.; Murray, A. J.; Parsons, R.; Pegg, D. J. *J. Electroanal. Chem.* **1996**, *409*, 51.
(41) Yagi, I.; Lantz, J. M.; Nakabayashi, S.; Corn, R.; Uosaki, K. *J. Electroanal. Chem.* **1996**, *401*, 95.
(42) Demir, U.; Shannon, C. *Langmuir* **1994**, *10*, 2794.
(43) Suggs, D. W.; Stickney, J. L. *Surf. Sci*. **1993**, *290*, 362.
(44) Hayden, B. E., Nandhakumar, I. S., to be published.
(45) Ikemiya, N. I.; Yamada, K.; Hara, S. *J. Vac. Sci. Technol.* **1996**, *B14*, 1369.